Draining and spreading along geometries that cause converging flows: Viscous gravity currents on a downward-pointing cone and a bowl-shaped hemisphere

Nan Xue and Howard A. Stone*
Department of Mechanical and Aerospace Engineering, Princeton University, Princeton, New Jersey 08544, USA

(Received 24 December 2020; accepted 30 March 2021; published 23 April 2021)

When a viscous liquid is released on an inclined solvophilic substrate, it spreads downwards by gravity and tends to coat the substrate. Here we report the gravitational axisymmetric spreading of a viscous liquid with a fixed volume on inclined geometries that cause converging flows, for example, on the inside of a downward-pointing hollow cone (funnel) and the lower part of a sphere (bowl). For the limit that the effect of surface tension is negligible, we analytically determine the thickness profile as well as the time-dependent position of the front of the spreading liquid. In the typical scenario that a liquid spreads on a geometry such as an inclined plate, the thickness of the front of the spreading liquid monotonically decreases in time throughout the spreading and a fingering instability occurs while the liquid film thins. However, we show that on an inclined geometry, where convergence of the flow occurs, the thickness of the spreading front first decreases in time and then increases. We also predict a critical volume V_c such that a fingering instability occurs if the volume of the spreading liquid is less than V_c. Experiments of axisymmetric spreading on a downward-pointing cone (funnel) are then performed and the measured position of the front and the critical liquid volume of the fingering instability agree with our theoretical predictions. This study highlights the effect of a geometry that focuses and thickens a thin film.

DOI: 10.1103/PhysRevFluids.6.043801

I. INTRODUCTION

A thin liquid film on an inclined substrate naturally drains and flows downwards due to the action of gravity. As a result, the liquid spreads on the substrate. These spreading flows are ubiquitous in industry and nature: for example, chocolate coating on a sphere [1], lava spreading over the surface of the Earth [2,3], or industrial wastewater slumping into a river [4]. Many examples of gravity currents are turbulent, especially when the liquid is of low viscosity (for example, water) and the scale of flow is large (for example, the breaking of a dam) [4–7]. However, in other common scenarios where the liquid is viscous or the scale of flow is sufficiently small, viscous effects dominate while inertial effects are often negligible, and lubrication theory can be applied to describe the spreading of the thin liquid film. Also, when the scale of the flow is much larger than the capillary length scale (usually of the order of magnitude of millimeters), the Bond number, which is the ratio of the gravitational forcing to the surface tension effects, is large, and the effect of surface tension on the macroscopic spreading is negligible.

Here we consider the gravitational spreading of a liquid in air. Note that for the system such as liquid spreading in another liquid, to describe the dynamics of the spreading, the gravitational acceleration g can be replaced by the reduced gravity $g' = (1 - \rho_2/\rho_1)g$, where ρ_1 and ρ_2 are,

*hastone@princeton.edu

respectively, the densities of the two liquids. One typical configuration of gravitational draining and spreading is the flow of a viscous gravity current on a two-dimensional slope (a flat inclined plate with infinite width) [8]. The thin film in air drains under the action of gravity, and the draining film thickness profile is self-similar as a function of position and time, which was first recognized by Jeffreys [9]. In particular, by balancing gravitational forcing and viscous effects, the thickness of the draining thin film is given by Jeffreys' solution

$$h_J(x,t) = \left(\frac{\nu x}{gt\sin\alpha}\right)^{1/2}, \tag{1}$$

where $\nu \equiv \mu/\rho$ is the kinematic viscosity of the liquid (μ is the dynamic viscosity of the liquid and ρ the density of the liquid), x the position along the film, t the time that the film drains, and α the inclination angle of the slope from the horizontal [8,9]. Note that Jeffreys considered the draining of a prewetted film, and Huppert appears to have been the first to recognize that, away from the contact line, the macroscopic film thickness profile of a gravitational spreading liquid on an inclined slope is identical to Jeffreys' solution [8]. For the case that the total volume of the liquid V is constant, the position of the front of the spreading film can be derived as

$$x_F(t) = \left(\frac{9A_0^2 gt\sin\alpha}{4\nu}\right)^{1/3}, \tag{2}$$

where $A_0 = V/w$ is the cross-sectional area of the liquid (w is the width of the liquid film on the inclined plate) and is conserved during the spreading according to the two-dimensional model. Substituting Eq. (2) into Eq. (1) shows that the film thickness of the spreading front $h_F(t) \propto t^{-1/3}$ [8] (to be concise, we denote the front of the spreading film as the *spreading front*). $h_F(t)$ decreases monotonically in time throughout the spreading.

In reality, the geometries of many substrates are complex. Besides the preceding example of spreading on an inclined plane, spreading on different geometries has been studied and reported: for example, spreading of a liquid on an upward-pointing cone [10], the top of a cylinder and a sphere [11], or a flexible beam [12]. In the former two cases, the spreading film drains similar to Jeffreys' solution, i.e., the film thickness $h \propto t^{-1/2}$. However, the film thickness as a function of the position $h(x,t)$, as well as the position of the spreading front as a function of time $x_F(t)$, are different in the different geometries. Table I provides a summary of the gravitationally driven film thickness profile and the position of the spreading front in the different geometries. Note that the gravitational spreading that we consider in this article is due to an inclined substrate, and the additional driving force from the variation of the film thickness is negligible, i.e., $\rho g\sin\alpha \gg \rho g|\nabla h|\cos\alpha$. In contrast, in other scenarios such as spreading on a horizontal substrate, the variation of the film thickness ∇h induces a pressure gradient in the liquid and thus drives the flow. Also, gravitational spreading can cause a flow to converge on horizontal geometries, for example, a liquid ring spreading inward on a horizontal plate. Often these gravity currents are self-similar, the spreading fronts are stable, and the film thickness monotonically decreases in time throughout the spreading [5,13–16].

When describing the gravitational spreading, the Bond number, which is the ratio of the gravitational forcing to the surface tension effects, is usually large, and therefore surface tension is negligible over much of the spreading film. However, typically, on millimeter or smaller length scales (the capillary length), surface tension plays a significant role connecting the front of the spreading film to the substrate. In the large Bond number limit, the macroscopic film thickness profile of the spreading liquid is determined by the gravitational drainage, except on the scale of the capillary length near the moving contact line. We denote the thickness of the spreading front, h_F, as the thickness of the spreading film at the end of the macroscopic gravitational draining region. Therefore, in the model below, the spreading film shape is governed by gravitational drainage until the film thickness $h = h_F$ near the spreading front, $x = x_F$, where surface tension becomes important and the film thickness becomes zero at the contact line. In addition, due to the effect of the surface tension near an advancing contact line, a fingering instability may occur when the

TABLE I. The film thickness profile and the position of the front of the liquid spreading on different geometries. Here R denotes the radius of the cylinder or the sphere, L and θ_0 denote the axisymmetric position where the liquid is released, θ denotes the angular position on the sphere, and α denotes the inclination angle of the float plate from the horizontal or the angle of the cone. The notation $\varphi(\theta) \equiv {}_2F_1(\frac{1}{2}, \frac{2}{3}; \frac{5}{3}; \sin^2\theta)$.

Geometry	Thickness profile (h)	Position of spreading front (x_F)	Reference
Flat inclined plate	$(\frac{\nu}{g\sin\alpha})^{1/2} x^{1/2} t^{-1/2}$	$(\frac{9gA^2\sin\alpha}{4\nu})^{1/3} t^{1/3}$	[8]
Cylinder (top)	$(\frac{3\nu R}{2g})^{1/2} t^{-1/2}$	$(\frac{gA^2}{6\nu R})^{1/2} t^{1/2}$	[11]
Upward-pointing cone	$(\frac{3\nu}{5g\cos\alpha})^{1/2} x^{1/2} t^{-1/2}$	$(\frac{125gV^2\cos\alpha}{48\pi^2\nu\sin^2\alpha})^{1/5} t^{1/5}$	[10] (exercise 7.12) & this work
Downward-pointing cone	$(\frac{3\nu}{5g\cos\alpha})^{1/2} [\frac{L^{5/3}}{(L-x)^{2/3}} - (L-x)]^{1/2} t^{-1/2}$	$L - [L^{5/3} - (\frac{125gV^2\cos\alpha}{48\pi^2\nu\sin^2\alpha})^{1/3} t^{1/3}]^{3/5}$	This work
Sphere (upper hemisphere)	$(\frac{3\nu R}{4g})^{1/2} t^{-1/2}$ (near the top)	$(\frac{4gV^2}{3\pi^2\nu R})^{1/4} t^{1/4}$	[11]
Sphere (bowl; near the bottom)	$(\frac{3\nu R}{4g})^{1/2} [\frac{\sin^{\frac{4}{3}}\theta_0}{\sin^{\frac{4}{3}}\theta} \varphi(\theta_0) - \varphi(\theta)]^{1/2} t^{-1/2}$	See Eq. (55)	This work
Flexible beam (note the imposed flow rate q at $x = 0$)		$\propto t^{4/5}$ (early times) $\propto t^4$ (intermediate times) $\propto t$ (late times)	[12]

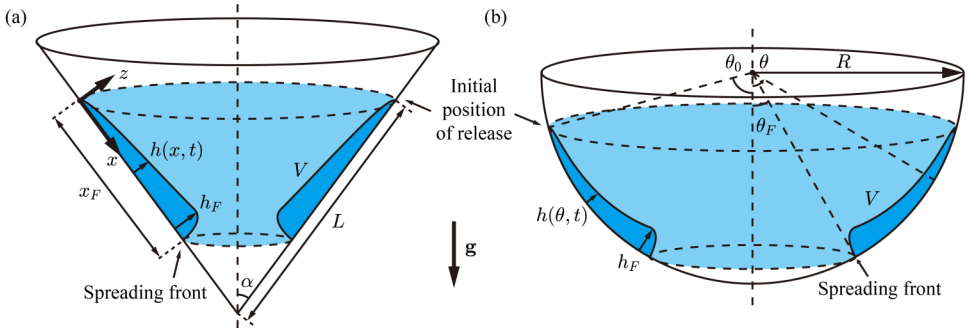

FIG. 1. Sketches of the gravitational spreading of a viscous liquid on inclined, converging geometries. (a) Spreading on a downward-pointing cone (funnel). (b) Spreading on the lower part of a sphere (bowl).

liquid spreads and thins, and the spreading front becomes unstable and splits into a series of rivulets [8,11,17–19]. The onset of the fingering instability is complex and has drawn significant attention. Generally, at the level of a scaling argument, on those geometries where the scale of the flow is larger than the capillary length ℓ_c (and the Bond number is large), a fingering instability occurs when the thickness of the spreading front h_F decreases to the order of magnitude of the capillary length ℓ_c [11,19–21]. At early times in many gravitationally driven thin film flows, the thickness of the spreading front is usually much thicker than the capillary length, and the spreading is stable; the film thins as it spreads, and during the late time, the thickness of the spreading front decreases in time and approaches to ℓ_c, and the spreading front becomes unstable and splits into many rivulets.

In this study, we report the gravitational spreading of a viscous Newtonian liquid with a fixed volume on inclined, geometries that cause a convergence, or focusing, of the flow, for example, on a downward-pointing cone (funnel) and on a bowl shape such as the lower half of a sphere; see the sketches in Fig. 1. Note that we consider the spreading on top of the geometries rather than under the geometries, where Rayleigh-Taylor instabilities (dripping) may occur [22–25]. For simplicity, we consider axisymmetric spreading, i.e., an axisymmetric ring of the liquid is released on the cone or the hemisphere and spreads. Breaking the symmetry will induce a new dimension into the problem [26,27], which is complex and we do not pursue it in this article. Starting with the lubrication theory, we derive the expressions for the characteristic features of the spreading thin film, such as the film thickness profile, the position of the spreading front, and the thickness of the spreading front. Typically, in the large Bond number limit of the previous studies (Table I), the thickness of the spreading front always monotonically decreases in time while the liquid spreads on the geometries. In contrast, in Secs. II, III, and IV, we show that for spreading over inclined, geometries where convergence of the flow occurs, there is the possibility to thicken the film height in time at the front so that the thickness of the spreading front first decreases in time and then increases during the spreading. This indicates that there is a minimum value of the thickness of the spreading front $h_{F,\min}$ during the spreading. $h_{F,\min}$ is also correlated to the critical volume of the liquid V_c that determines whether a fingering instability will occur on a given geometry, and we also estimate V_c. Finally, experiments of axisymmetric spreading on a downward-pointing cone are performed. The position of the spreading front as a function of time as well as the critical liquid volume V_c for fingering to occur are measured, and the results are in agreement with our predictions.

II. AXISYMMETRIC SPREADING ON A DOWNWARD-POINTING CONE

In this section, we consider the axisymmetric gravitational spreading of a viscous Newtonian liquid on a downward-pointing cone (funnel), with the cone angle α; see the sketch in Fig. 1(a). Initially, at time $t = 0$, an axisymmetric ring of the liquid with a total volume of V is released on the cone, where the distance between the liquid ring and the vertex of the cone along the generatrix

is L. The released liquid then spreads toward the vertex of the cone under the action of gravity. We denote the direction along the generatrix of the cone as x and the direction orthogonal to the surface of the cone as z, where $x = 0$ represents the initial position of the liquid that is released and $z = 0$ represents the surface of the cone. We assume that the top contact line at $x = 0$ remains pinned throughout the spreading, the spreading of the liquid is axisymmetric, and the spreading front is stable (no fingering instability occurs). The thickness profile of the spreading thin film is denoted as $h(x, t)$. The position of the spreading front is denoted as $x_F(t)$ and the film thickness at the spreading front is denoted as $h_F(x_F)$ or $h_F(t)$.

In the setup of the mathematical model, the liquid with a total volume of V is released from $x = 0$ at time $t = 0$, which indicates that all the liquid is accumulated at a singular position (at a singular circle on the cone) and the film thickness profile behaves like a singular δ-function shape. We note that this initial setup in the model is for theoretical convenience of the mathematical derivation but is not applicable in real experiments. In the experiments, the liquid is released on the geometry at time τ (τ denotes the time in the experiments, while t denotes the time in the model) and already occupies a certain amount of area on the geometry. As a result, unlike the singular film shape in the model, there is an effect of the initial shape of the liquid film in the experiments. Note that in this article, as with many studies of film spreading, we focus on the asymptotic properties of the spreading film, when the spreading time of the liquid film is so long that the film has no record/memory of its initial shape. In this limit, the correlation between the time τ in the experiment and the time t in the model can be given as $t = \tau + t_s$, where t_s is the shift of time (due to the effect of the initial film shape) between the experiment and the model. The property of t_s will be further discussed in Sec. IV C. In the modeling sections below (Secs. II and III), we consider that $t \gg t_s$, i.e., the initial effect is negligible, and we will only use t throughout the model.

A. Film thickness profile

We first study the thickness profile of the spreading film $h(x, t)$. Generally, the spreading of the thin film is affected by the gravitational forcing and the surface tension. In the lubrication approach, the mean curvature of the interface of the thin film is approximately

$$\kappa = \frac{1}{2}\left(\frac{\partial^2 h}{\partial x^2} + \frac{1}{(L-x)\tan\alpha}\right). \tag{3}$$

Note that $\frac{\partial^2 h}{\partial x^2}$ and $\frac{1}{(L-x)\tan\alpha}$ are, respectively, the two principal curvatures of the thin film on the cone. This estimate breaks down where $h \approx (L - x)\tan\alpha$ (when the spreading front approaches to the vertex of the cone). The mean curvature of the interface κ generates a pressure difference, i.e., the Laplace pressure $p_\gamma = -2\gamma\kappa$, across the interface of the thin film to the atmosphere, where γ is the surface tension of the liquid.

To describe the incompressible flow, we assume that the velocity is approximately unidirectional, i.e., $\mathbf{u} \approx u\mathbf{e}_x$. The equation of the velocity u along the viscous thin film flow is

$$\mu\frac{\partial^2 u}{\partial z^2} + \rho g\cos\alpha + \rho g\sin\alpha\frac{\partial h}{\partial x} + \gamma\frac{\partial}{\partial x}\left(\frac{\partial^2 h}{\partial x^2} + \frac{1}{(L-x)\tan\alpha}\right) = 0. \tag{4}$$

We consider the scenario that the effect of surface tension is negligible when macroscopically describing the gravitational spreading (the effect of surface tension will be discussed in Sec. II C), i.e., the Bond number,

$$\mathrm{Bo} \equiv \rho g V/\gamma L \gg 1. \tag{5}$$

We also consider that $\rho g\cos\alpha \gg \rho g\sin\alpha|\frac{\partial h}{\partial x}|$, i.e., the gravitational driving force from the variation of the film thickness is negligible. Note that approximately $|\partial h/\partial x| = O(10^{-2}) \ll 1$ in the experiments presented in Sec. IV. In these limits, the pressure is uniform along the flow direction and

Eq. (4) becomes

$$\mu \frac{\partial^2 u}{\partial z^2} + \rho g \cos\alpha = 0. \tag{6}$$

Applying the boundary conditions that $u = 0$ at $z = 0$ (no slip) and $\partial u/\partial z = 0$ at $z = h$ (stress-free interface), the velocity profile along the film is

$$u = \frac{g\cos\alpha}{\nu}\left(hz - \frac{1}{2}z^2\right). \tag{7}$$

Note that the perimeter of a ring of the liquid at x is $2\pi(L - x)\sin\alpha$ and is one of the key features of the geometry [Fig. 1(a)]. With the velocity profile, the flow rate of the liquid ring is

$$q(x, t) = 2\pi(L - x)\sin\alpha \int_0^h u\mathrm{d}z = \frac{2\pi g \sin\alpha\cos\alpha}{3\nu} h^3(L - x). \tag{8}$$

The variation in time of the film thickness h is directly induced by the gradient of the flow rate $\partial q/\partial x$, i.e., for this geometry the continuity equation has the form

$$2\pi(L - x)\sin\alpha \frac{\partial h}{\partial t} = -\frac{\partial q}{\partial x} = -\frac{2\pi g \sin\alpha\cos\alpha}{3\nu} \frac{\partial[h^3(L - x)]}{\partial x}. \tag{9}$$

Equation (9) is a first-order partial differential equation (PDE) for $h(x, t)$, and can be simplified as

$$\frac{\partial h}{\partial t} = -\frac{g\cos\alpha}{3\nu(L - x)} \frac{\partial[h^3(L - x)]}{\partial x}. \tag{10}$$

Note that close to the initial position of release, in the limit of $x \ll L$, the film has no knowledge of the geometry of the cone and the dynamics is identical to the spreading on a 2D slope [8,9]. In this limit, Eq. (10) has a self-similar solution identical to Eq. (1). However, beyond this limit, there is a given length scale L in this cone geometry and thus the solution of Eq. (10) would not be the same as Eq. (1). To make the equations nondimensional [7], it is convenient to introduce the scales of the film thickness, the flow velocity, and the time of spreading as

$$h_0 = \frac{V}{\pi L^2 \sin\alpha}, \quad u_0 = \frac{g h_0^2 \cos\alpha}{3\nu} = \frac{g V^2 \cos\alpha}{3\pi^2 \nu L^4 \sin^2\alpha}, \quad t_0 = \frac{L}{u_0} = \frac{3\pi^2 \nu L^5 \sin^2\alpha}{g V^2 \cos\alpha}, \tag{11}$$

where h_0 is the scale of the spreading film thickness (note that $\pi L^2 \sin\alpha$ is the lateral surface area of the cone), u_0 is the scale of the flow velocity in the film, and t_0 is the scale of the spreading time of the film. Note that the Reynolds number

$$\mathrm{Re} = \frac{u_0 h_0}{\nu} = \frac{g V^3 \cos\alpha}{3\pi^3 \nu^2 L^6 \sin^3\alpha}. \tag{12}$$

Substituting the characteristic parameters in our experiments (Sec. IV), $V = 300\ \mathrm{cm}^3$, $\alpha = 30$ degrees, $\mu = 40$ Pa s, $\rho = 1.4 \times 10^3\ \mathrm{kg/m}^3$, and $L = 25$ cm, the estimated $\mathrm{Re} = O(10^{-4}) \ll 1$. The effect of inertia is therefore negligible. Moreover, in lubrication situations, the effective Reynolds number comparing inertial to viscous terms in the Navier-Stokes equation is $\mathrm{Re}_{\mathrm{eff}} = \mathrm{Re} h_0/L$, which is even smaller than Re. Note that to estimate the Reynolds number at the beginning of the spreading, rather than using h_0, it is more reasonable to estimate a length $\ell = [V/(2\pi L \sin\alpha)]^{1/2}$, and the corresponding Reynolds number $\mathrm{Re} = \frac{g\ell^3\cos\alpha}{3\nu^2} = O(10^{-2})$.

With the typical scales identified here [Eq. (11)], the corresponding dimensionless expression for the (film) length, film thickness, and the time of spreading are, respectively,

$$X = \frac{x}{L}, \quad H = \frac{h}{h_0}, \quad T = \frac{t}{t_0}. \tag{13}$$

Substituting Eqs. (11) and (13) into the PDE for $h(x,t)$ [Eq. (10)], the dimensionless expression for the governing equation of the film thickness is

$$\frac{\partial H}{\partial T} = -\frac{1}{1-X}\frac{\partial[H^3(1-X)]}{\partial X}. \tag{14}$$

We focus on the long-time features of the spreading film, when the effect of the initial shape of the liquid film is negligible, i.e., $t \gg t_s$. Note that in the governing equation [Eq. (14)], time T only enters through a time derivative, and therefore there is a freedom to shift the origin of time, i.e., to apply $t = \tau + t_s$. This shift of time will be further discussed in Sec. IV C. We assume that the film thickness profile $h(x,t)$ [or $H(X,T)$] is self-similar with time t (or T), so that Eq. (14) admits a solution

$$H(X,T) = \mathcal{H}(X)T^{-1/2}, \tag{15}$$

where $\mathcal{H}(X)$ is a function that describes the film thickness profile and is only dependent on the independent variable X. Substituting Eq. (15) into Eq. (14), the PDE for $H(X,T)$ becomes an ODE for $\mathcal{H}(X)$,

$$\frac{1}{2}(1-X)\mathcal{H} = \frac{d}{dX}[(1-X)\mathcal{H}^3]. \tag{16}$$

The boundary condition for Eq. (16) is $\mathcal{H}(0) = 0$ (the film thickness is zero at the contact line, i.e., $h = 0$ at $x = 0$).

The general solutions of Eq. (16) are

$$\mathcal{H} = 0 \quad \text{or} \quad \mathcal{H} = \pm\left[\frac{c}{(1-X)^{2/3}} + \frac{X}{5} - \frac{1}{5}\right]^{1/2}, \tag{17}$$

where c is a constant and the desired solution is positive. Applying the boundary condition, the constant $c = \frac{1}{5}$. Therefore, the solution of Eq. (16) is

$$\mathcal{H}(X) = \frac{1}{\sqrt{5}}\left[\frac{1}{(1-X)^{2/3}} + X - 1\right]^{1/2}. \tag{18}$$

Note that for small X (close to $X = 0$),

$$\mathcal{H}(X) = \frac{1}{\sqrt{3}}X^{1/2} + O(X^{3/2}). \tag{19}$$

This asymptotic property of $\mathcal{H}(X)$ close to $X = 0$ agrees with Jeffreys' solution $h_J \propto x^{1/2}$, as noted above.

Substituting Eq. (18) into Eq. (15), the dimensionless expression for the film thickness is

$$H(X,T) = \frac{1}{\sqrt{5}}\left[\frac{1}{(1-X)^{2/3}} + X - 1\right]^{1/2} T^{-1/2}. \tag{20}$$

The corresponding dimensional expression for the film thickness $h(x,t)$ is

$$h(x,t) = \left(\frac{3\nu L}{5g\cos\alpha}\right)^{1/2}\left[\frac{1}{\left(1-\frac{x}{L}\right)^{2/3}} - \left(1-\frac{x}{L}\right)\right]^{1/2} t^{-1/2}, \tag{21}$$

which highlights the features of the film thickness profile: (1) at a fixed position, the thickness of the thin film decreases in time while spreading and draining, following the power law $h \propto t^{-1/2}$, similar to Jeffreys' solution; and (2) at a given time, within the spreading film ($x \leqslant x_F$), the film is thicker away from the initial position of release; see $\mathcal{H}(X)$ in Fig. 2(a). Close to $X = 0$, the initial position where the liquid is released, $\mathcal{H}(X)$ is close to the film structure on a 2D slope. However, away from the top contact line $X = 0$, $\mathcal{H}$ increases more rapidly than on a 2D slope or on an upward-pointing

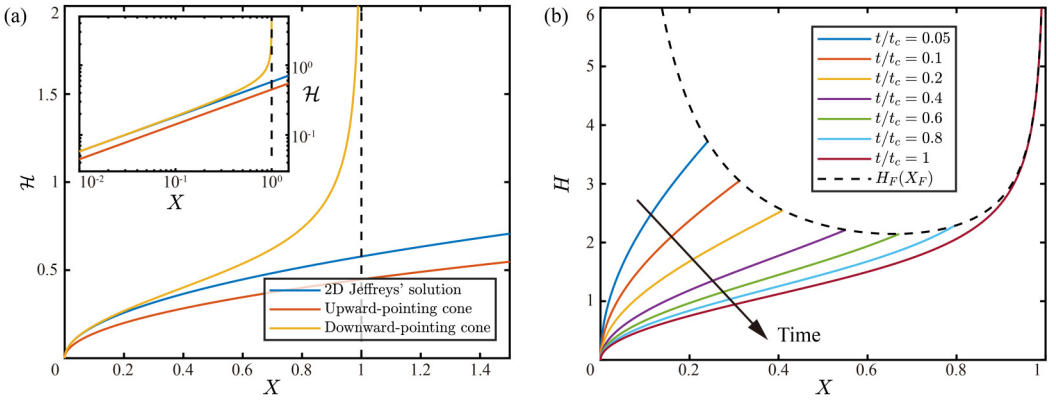

FIG. 2. (a) The dimensionless film thickness profile function $\mathcal{H}$ as a function of X; Eq. (18). The inset shows $\mathcal{H}(X)$ with logarithmic axes. The blue, red, and yellow lines shows the film shape function $\mathcal{H}$ of spreading on a 2D slope, an upward-pointing cone, and a downward-pointing cone, respectively. To compare, we set a length scale L and a timescale t_0 according to Eq. (11) in all these geometries to find $\mathcal{H}(X)$ so that the film thickness profile satisfies Eq. (15). (b) The time development of the film thickness profile while the liquid spreads on a downward-pointing cone. The scaled film thickness H as a function of the scaled position X is displayed. The solid lines show the thickness profile of the spreading film with different times, from $t/t_c = 0.05$ to 1 [t_c is the amount of time that the film spreads from the initial position of release $x_F = 0$ to the vertex of the cone $x_F = L$; see the definition of t_c in Eq. (25)]. The dashed line shows the thickness of the spreading front H_F as a function of the position of the spreading front X_F.

cone (see the derivations in the Appendix A). These different properties of the film structure $\mathcal{H}$ on the downward-pointing cone are due to the converging flow: as the thin film gets closer to the vertex of the cone, the perimeter of the liquid ring becomes smaller, and therefore the draining liquid converges and thickens. Note that near the vertex of the cone $X = 1$, the opposite sides of the liquid interface will collide as $\mathcal{H}$ sharply increases.

The rapid increase of $\mathcal{H}$ with X indicates that the thickness of the front of the spreading film may also increase as the spreading front approaches the vertex of the cone. Our next goal is to find expressions for the position as well as the thickness of the spreading front.

B. Front of the thin film

While the thin film spreads on the downward-pointing cone, the film thickness profile is given by Eq. (21) from the top contact line (initial position where the liquid is released, $x = 0$) to the end of the spreading front $x = x_F(t)$, where the film thickness profile steeply changes from the global profile [Eq. (21)] to zero at the contact line under the action of surface tension. In the limit of large Bond number, this capillary region of steep transition is much smaller than the macroscopic scale of the spreading film and we neglect its contribution to the volume of the film [8,20]. A scaling argument for the scale of this capillary region will be given in the next section (Sec. II C). The total volume of the liquid V is constant throughout the spreading, thus

$$\int_0^{x_F(t)} 2\pi \sin\alpha (L - x) h(x,t) dx = V. \tag{22}$$

Substituting the expression for $h(x,t)$ [Eq. (21)] into Eq. (22), we can derive the position of the spreading front as a function of time. The result is

$$\frac{x_F(t)}{L} = 1 - \left[1 - \left(\frac{125 g V^2 \cos\alpha}{48\pi^2 \nu L^5 \sin^2\alpha}\right)^{1/3} t^{1/3}\right]^{3/5}, \tag{23}$$

and the dimensionless expression for $X_F(T)$ is

$$X_F(T) = 1 - \left[1 - \left(\frac{125T}{16}\right)^{1/3}\right]^{3/5}, \tag{24}$$

where $X_F \equiv x_F/L$, and is the dimensionless position of the spreading front. The expression for $x_F(t)$ [Eq. (23)] indicates that the timescale of the liquid spreading is

$$t_c = \frac{48\pi^2 \nu L^5 \sin^2\alpha}{125 g V^2 \cos\alpha}. \tag{25}$$

Here t_c is the time to spread from the initial position of release ($x = 0$) to the vertex of the cone ($x = L$). The dimensionless expression for the spreading time t_c is

$$T_c \equiv \frac{t_c}{t_0} = \frac{16}{125}. \tag{26}$$

It is also straightforward to substitute the expression for $x_F(t)$ [Eq. (23)] into the film thickness profile $h(x,t)$ [Eq. (21)] to obtain the thickness of the front of the spreading film. As a result,

$$h_F(x_F) = \frac{5V}{4\pi \sin\alpha} \frac{1}{(L - x_F)^{1/3}[L^{5/3} - (L - x_F)^{5/3}]}. \tag{27}$$

The dimensionless expression for h_F is

$$H_F(X_F) = \frac{5}{4(1 - X_F)^{1/3}[1 - (1 - X_F)^{5/3}]}, \tag{28}$$

where $H_F \equiv h_F/h_0$, and is the dimensionless thickness of the spreading front.

With the knowledge of $x_F(t)$ [Eq. (23)], the structure of the film thickness profile throughout the spreading can be constructed; see the time development of the scaled film thickness profile as a function of the scaled position plotted in Fig. 2(b). Throughout the spreading, the film thickness profile follows the expression for $h(x,t)$ [Eq. (21)] from the top of the contact line ($x = 0$) to the spreading front ($x = x_F$). As a result, the film thickness at a fixed position monotonically decreases in time due to the gravitational drainage. However, unlike the spreading on a 2D slope ($h_F \propto x_F^{-1}$) or on an upward-pointing cone ($h_F \propto x_F^{-2}$), the thickness of the spreading front h_F does not monotonically decrease in time during the spreading on a downward-pointing cone: h_F first decreases and then increases with x_F [the dashed line in Fig. 2(b); see also the yellow solid line in Fig. 3(a)] due to the converging flow. In addition, we note that when the spreading liquid approaches the vertex of the cone ($x_F/L \to 1$), the spreading front is so thick [$h_F \sim (L - x_F)\tan\alpha$] that opposite sides collide and the whole film is expected to coalesce. Also, when the slope of the spreading front interface is too steep, lubrication theory breaks down and the expression for $x_F(t)$ [Eq. (23)] is no longer valid. This breakdown only occurs when the spreading front is very close to the vertex of the cone, but this is not the major topic in our model.

Another signature of the spreading is the position of the spreading front as a function of time, $x_F(t)$ [Eq. (23)]; see the yellow line in Fig. 3(b). Note that scaled by t_c [Eq. (25)], the relationships of the position of the spreading front as a function of time are simply $x_F/L = \frac{3}{5}(t/t_c)^{1/3}$ on a 2D slope [the blue line in Fig. 3(b); note that we set $A = V/(2\pi L \sin\alpha)$] and $x_F/L = (t/t_c)^{1/5}$ on an upward-pointing cone [the red line in Fig. 3(b)]. For the spreading on a 2D slope or on an upward-pointing cone, the speed of the spreading front monotonically decreases in time as the liquid spreads; for the spreading on a downward-pointing cone, the speed of the spreading front decreases initially ($t/t_c \lesssim 0.2$), but then remains approximately constant ($0.2 \lesssim t/t_c \lesssim 0.8$), which is due the fact that the spreading liquid is focused by the geometry. Measuring and comparing $x_F(t)$ with these predictions will be the focus of our experiments. It is also interesting but not intuitive that the spreading of a ring of liquid to the vertex on a downward-pointing cone takes the same period of time as the spreading of the same amount of liquid from the vertex to the ring on an upward-pointing cone

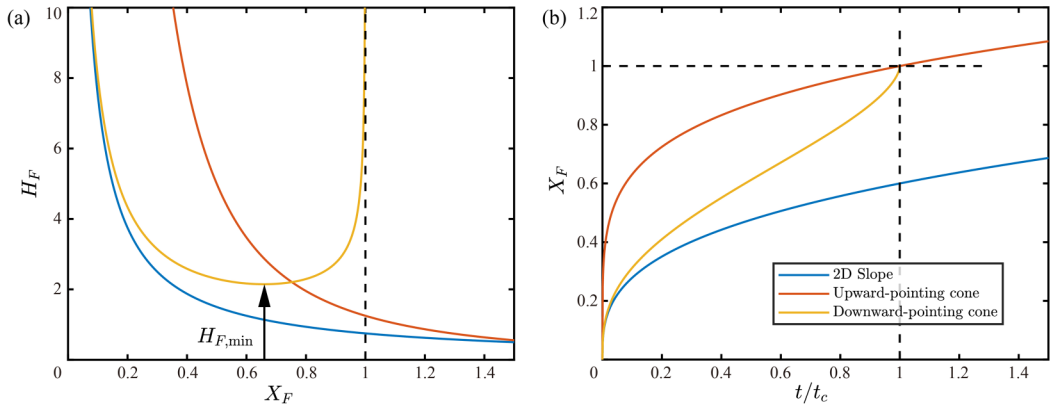

FIG. 3. (a) The scaled thickness of the spreading front H_F as a function of the scaled spreading distance X_F. The blue, red and yellow lines, respectively, show the spreading on a 2D slope, an upward-pointing cone and a downward-pointing cone. (b) The scaled spreading distance of the film X_F as a function of the scaled time t/t_c.

[the red line and the yellow line in Fig. 3(b) meet at $x_F/L = 1$ and $t/t_c = 1$]. The position of the spreading front as a function of time $x_F(t)$ will be examined later in the experiments of spreading on a downward-pointing cone in Sec. IV.

C. A capillary region where surface tension matters

In the preceding Sec. II B, we described that near $x = x_F(t)$ the film thickness steeply changes from $h_F(x_F)$ to zero due to the action of surface tension. Here we make a scaling argument to estimate the scale of this capillary region where surface tension is significant (e.g., see Ref. [8]). We start from Eq. (4), the equation for the velocity u along the viscous thin film flow. We consider that $\rho g\cos\alpha \gg \rho g\sin\alpha|\frac{\partial h}{\partial x}|$, and the equation of the velocity u is

$$\mu\frac{\partial^2 u}{\partial z^2} + \rho g\cos\alpha + \gamma\frac{\partial}{\partial x}\left(\frac{\partial^2 h}{\partial x^2} + \frac{1}{(L-x)\tan\alpha}\right) = 0. \tag{29}$$

Applying the boundary conditions ($u = 0$ at $z = 0$ and $\partial u/\partial z = 0$ at $z = h$), the velocity profile is

$$u = \frac{1}{\mu}\left(hz - \frac{1}{2}z^2\right)\left[\rho g\cos\alpha + \gamma\frac{\partial}{\partial x}\left(\frac{\partial^2 h}{\partial x^2} + \frac{1}{(L-x)\tan\alpha}\right)\right]. \tag{30}$$

With this velocity profile, the flow rate at x is

$$q(x,t) = \frac{2\pi\sin\alpha}{3\mu}h^3(L-x)\left[\rho g\cos\alpha + \gamma\frac{\partial}{\partial x}\left(\frac{\partial^2 h}{\partial x^2} + \frac{1}{(L-x)\tan\alpha}\right)\right], \tag{31}$$

and the continuity equation becomes

$$3\mu\frac{\partial h}{\partial t} + \frac{1}{L-x}\frac{\partial}{\partial x}\left\{h^3(L-x)\left[\rho g\cos\alpha + \gamma\frac{\partial}{\partial x}\left(\frac{\partial^2 h}{\partial x^2} + \frac{1}{(L-x)\tan\alpha}\right)\right]\right\} = 0. \tag{32}$$

Equation (32) is the PDE for the film thickness $h(x,t)$ where the effect of surface tension is considered. The three terms in Eq. (32) are, respectively, the viscous term, the gravitational spreading term, and the surface tension term. A complete form of the governing equation of the film thickness profile can be found in Ref. [19]. Note that near the spreading front, we assume that the mean curvature of the thin film is much larger than the curvature of geometry, i.e., $|\kappa| \gg \frac{1}{(L-x)\tan\alpha}$. In this

limit, $\kappa = \frac{1}{2}\frac{\partial^2 h}{\partial x^2}$. Eq. (32) becomes

$$3\mu\frac{\partial h}{\partial t} + \frac{1}{L-x}\frac{\partial}{\partial x}\left[h^3(L-x)\left(\rho g\cos\alpha + \gamma\frac{\partial^3 h}{\partial x^3}\right)\right] = 0. \tag{33}$$

Rather than fully solving Eq. (33) analytically or numerically, we are interested in a scaling argument for the length scale of the region where surface tension is significant. We denote the length scale of this boundary-layer-type region as ξ_0. Near the spreading front, the viscous term $\partial h/\partial t$ is assumed to be negligible and the surface tension term balances with the gravitational spreading term. In this capillary region, the film thickness steeply changes from h_F to zero, and therefore

$$\rho g\cos\alpha \sim \gamma\frac{\partial^3 h}{\partial x^3} \sim \gamma\frac{h_F}{\xi_0^3}. \tag{34}$$

Thus, the length scale of this capillary region is

$$\xi_0 = \left(\frac{\gamma h_F}{\rho g\cos\alpha}\right)^{1/3}. \tag{35}$$

This expression for $\xi_0(h_F)$ is the same as reported by Huppert [8]. In particular, substituting the characteristic parameters in our experiments (Sec. IV), $\gamma = 86$ mN/m, $h_F = 5$ mm, $\rho = 1.4 \times 10^3$ kg/m^3, and $\alpha = 30$ degrees, the resulting $\xi_0 = 3.3$ mm and is much smaller than the size of the geometry (tens of centimeters in our experiments). Also, when the fingering instability occurs, $h_F \sim \ell_c = 2.5$ mm, and the corresponding $\xi_0 = 2.6$ mm.

Note that the thickness of the spreading front h_F scales with h_0, and according to the scaling argument [Eq. (11)],

$$\xi_0 \sim \left(\frac{\gamma V}{\pi\rho g L^2\sin\alpha\cos\alpha}\right)^{1/3}. \tag{36}$$

A more detailed discussion about the capillary region and the fingering instability of a viscous liquid film spreading on a funnel can be found in Ref. [19].

D. Critical liquid volume of fingering instabilities

While the liquid spreads on a downward-pointing cone under the action of gravity, the thickness of the spreading front first decreases and then increases in time [Fig. 3(a), Eqs. (23) and (27)]. This indicates that there is a minimum value of the thickness of the spreading front during the spreading. From Eq. (27), the minimum value of the spreading front thickness is

$$h_{F,\min} = \frac{3\sqrt[5]{6}V}{2\pi L^2\sin\alpha}, \tag{37}$$

and the corresponding position of the spreading front where the minimum occurs is

$$x_{F,\min} = \left(1 - 6^{-3/5}\right)L \approx 0.6587L. \tag{38}$$

As a result, during the spreading, the thickness of the spreading front monotonically decreases in time until it reaches the minimum $h_{F,\min}$ at $x_F = x_{F,\min}$ and then monotonically increases in time. Further, $h_{F,\min}$ is related to whether the fingering instability would occur during the spreading. Using a scaling argument described in the introduction, the spreading front becomes unstable and splits into a series of rivulets when the thickness of the spreading front h_F decreases to the order of magnitude of the capillary length ℓ_c, i.e., $h_F \sim \ell_c$ [11,20,21]. Following this argument, for the spreading on a downward-pointing cone, we expect that the spreading front is stable for $h_{F,\min} \gtrsim \ell_c$ and a fingering instability is predicted for $h_{F,\min} \lesssim \ell_c$. According to Eq. (37), the corresponding

critical total volume of the liquid is

$$V_c \sim \frac{2\pi L^2 \ell_c \sin\alpha}{3\sqrt[5]{6}}. \tag{39}$$

When the total volume of the liquid $V > V_c$, the spreading front is stable throughout the spreading, since the thickness of the spreading front in the gravitationally controlled region is always thicker than the order of magnitude of ℓ_c; in contrast, when $V < V_c$, a fingering instability occurs when the thickness of the spreading front decreases to the order of magnitude of ℓ_c. This critical liquid volume for the fingering instability will be examined later in the experiments in Sec. IV.

III. AXISYMMETRIC SPREADING ON A BOWL-SHAPED HEMISPHERE

In this section, we consider the axisymmetric gravitational spreading of a viscous Newtonian liquid inside and on a bowl, for example, as presented by the lower half of a hemisphere; see the sketch in Fig. 1(b). The radius of the hemisphere is R. We denote the angle of the position on the hemisphere to the axis of symmetry as θ. Initially, at $t = 0$, an axisymmetric ring of the liquid with a volume of V is released on the hemisphere, from an angle of θ_0, where $\theta = 0$ represents the bottom of the hemisphere. The released liquid spreads toward the bottom of the hemisphere due to the action of gravity and we assume that the spreading is axisymmetric and no fingering instability occurs. The top contact line at $\theta = \theta_0$ is pinned throughout the spreading. The thickness profile of the spreading thin film is denoted as $h(\theta, t)$. The position of the spreading front is denoted as $\theta_F(t)$ and the thickness of the spreading front is denoted as $h_F(\theta_F)$. Our goal is to find the expressions for $h(\theta, t)$, $\theta_F(t)$ and $h_F(\theta_F)$; the derivations are similar to those in the preceding section.

A. Film thickness profile

We consider that the thickness of the film is much smaller than the scale of the hemisphere, $h \ll R$. The lubrication approximation means that the flow profile is unidirectional and parabolic. The velocity profile along the film is

$$u = \frac{g\sin\theta}{\nu}\left(hz - \frac{1}{2}z^2\right). \tag{40}$$

Here z is orthogonal to the surface of the sphere and directed to the center of the sphere. This velocity profile is also identical to the velocity profile along the spreading film on an upper hemisphere [11].

The perimeter of a liquid ring at θ is $2\pi R\sin\theta$ [Fig. 1(b)]. The corresponding flow rate of the liquid ring at θ is

$$q(\theta, t) = 2\pi R\sin\theta \int_0^h u dz = \frac{2\pi gR}{3\nu} h^3 \sin^2\theta. \tag{41}$$

Applying the continuity equation, the PDE of the film thickness $h(\theta, t)$ is

$$\frac{\partial h}{\partial t} = \frac{g}{3\nu R\sin\theta} \frac{\partial (h^3 \sin^2\theta)}{\partial \theta}. \tag{42}$$

As for a scaling argument [7], similar to Sec. II A, it is convenient to introduce the scales of the film thickness, the flow velocity, and the time of spreading as

$$h_0 = \frac{V}{2\pi R^2}, \quad u_0 = \frac{gh_0^2}{3\nu} = \frac{gV^2}{12\pi^2 \nu R^4}, \quad t_0 = \frac{R}{u_0} = \frac{12\pi^2 \nu R^5}{gV^2}. \tag{43}$$

The corresponding dimensionless expression for the film thickness and the time of the spreading are, respectively,

$$H = \frac{h}{h_0}, \quad T = \frac{t}{t_0}. \tag{44}$$

Substituting Eqs. (43) and (44) into the PDE for $h(\theta, t)$ [Eq. (42)], the dimensionless expression for governing equation of the film thickness is

$$\frac{\partial H}{\partial T} = \frac{1}{\sin\theta}\frac{\partial(H^3\sin^2\theta)}{\partial\theta}. \tag{45}$$

Neglecting the effect of the initial shape of the liquid, i.e., $t \gg t_s$, we can convert Eq. (45) from a time-dependent PDE to an ODE by assuming

$$H(\theta, T) = \mathcal{H}(\theta)T^{-1/2}, \tag{46}$$

which is similar to Eq. (15). Here $\mathcal{H}(\theta)$ describes the film thickness profile and is only dependent on θ. Substituting Eq. (46) into Eq. (45), we get a dimensionless form of the ODE for the film thickness profile,

$$\frac{1}{2}\mathcal{H}\sin\theta + \frac{d}{d\theta}(\mathcal{H}^3\sin^2\theta) = 0. \tag{47}$$

The boundary condition for Eq. (47) is $\mathcal{H}(\theta_0) = 0$, i.e., the film thickness h is zero at $\theta = \theta_0$ (the initial position of release). The solutions of Eq. (47) are (we use Mathematica and follow their notation for the generalized hypergeometric function ${}_pF_q$)

$$\mathcal{H} = 0 \quad \text{or} \quad \mathcal{H} = \pm\frac{1}{2}\left[\frac{c}{\sin^{\frac{4}{3}}\theta} - {}_2F_1\left(\frac{1}{2}, \frac{2}{3}; \frac{5}{3}; \sin^2\theta\right)\right]^{1/2} \equiv \pm\frac{1}{2}\left[\frac{c}{\sin^{\frac{4}{3}}\theta} - \varphi(\theta)\right]^{1/2}, \tag{48}$$

where c is a constant, and we introduce a notation $\varphi(\theta) \equiv {}_2F_1(\frac{1}{2}, \frac{2}{3}; \frac{5}{3}; \sin^2\theta)$ for simplification. We seek a positive solution for the film thickness. Applying the boundary condition, the constant is

$$c = \sin^{\frac{4}{3}}\theta_0\varphi(\theta_0). \tag{49}$$

Therefore,

$$\mathcal{H}(\theta) = \frac{1}{2}\left[\frac{\sin^{\frac{4}{3}}\theta_0}{\sin^{\frac{4}{3}}\theta}\varphi(\theta_0) - \varphi(\theta)\right]^{1/2}. \tag{50}$$

Note that for small $\theta_0 - \theta$,

$$\mathcal{H}(\theta) = \left(\frac{\theta_0 - \theta}{3\sin\theta_0}\right)^{1/2} + O\big[(\theta_0 - \theta)^{3/2}\big]. \tag{51}$$

This asymptotic property of $\mathcal{H}(\theta)$ agrees with Jeffreys' solution [Eq. (1)]. Substituting Eq. (50) into Eq. (46), the dimensionless form of the film thickness profile is

$$H(\theta, T) = \frac{1}{2}\left[\frac{\sin^{\frac{4}{3}}\theta_0}{\sin^{\frac{4}{3}}\theta}\varphi(\theta_0) - \varphi(\theta)\right]^{1/2} T^{-1/2}. \tag{52}$$

The corresponding dimensional form of the film thickness profile is

$$h(\theta, t) = \left(\frac{3\nu R}{4g}\right)^{1/2}\left[\frac{\sin^{\frac{4}{3}}\theta_0}{\sin^{\frac{4}{3}}\theta}\varphi(\theta_0) - \varphi(\theta)\right]^{1/2} t^{-1/2}. \tag{53}$$

The structure of the film thickness profile $\mathcal{H}$ as a function of θ is shown in Fig. 4. The initial position of release θ_0 affects the value of $\mathcal{H}(\theta)$ [Fig. 4(a)], but the shape of $\mathcal{H}$ with different θ_0 is similar: close to the initial position of release, the film thickness profile is similar to Jeffreys' solution [Fig. 4(b)] and follows Eq. (51); the film thickness monotonically increases with $\theta_0 - \theta$, and the increase becomes more rapid when approaching to the bottom of the hemisphere, since the liquid is focused by the geometry while the perimeter of the liquid ring decreases. Note that the film thickness becomes singular at $\theta = 0$. We note that close to the bottom, the limit $(1/R)|dh/d\theta| \ll 1$

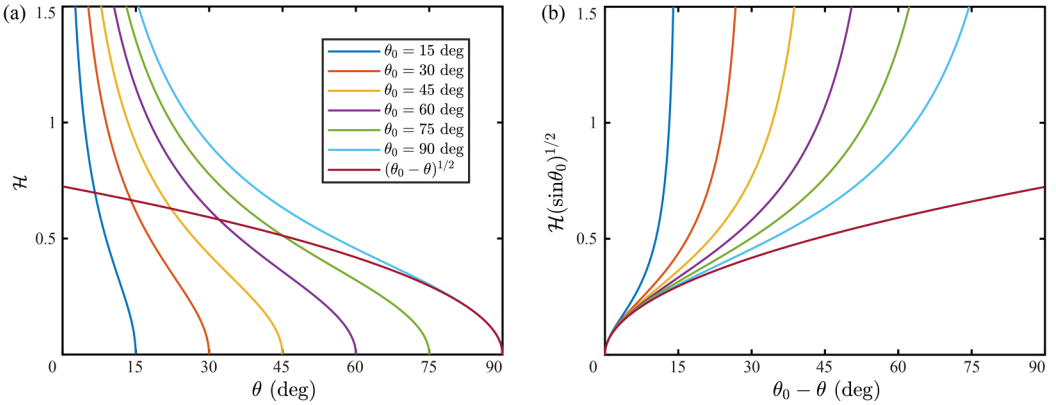

FIG. 4. Film thickness profile as a function of θ or $\theta_0 - \theta$, with different initial angle θ_0; Eq. (50).

breaks down so that the film thickness profile deviates from Eq. (53); this only occurs when the film is very close to the bottom of the hemisphere.

B. Front of the thin film

The film thickness profile is Eq. (53) from $\theta = \theta_0$ to $\theta = \theta_F$. Since the total volume of the liquid V is constant during the spreading,

$$\int_{\theta_F(t)}^{\theta_0} 2\pi R^2 \sin\theta h(\theta, t) d\theta = V. \tag{54}$$

By substituting Eq. (53) into Eq. (54) and simplifying, we get

$$t = \frac{3\pi^2 \nu R^5}{gV^2} \left\{ \int_{\theta_F(t)}^{\theta_0} \sin\theta \left[\frac{\sin^{\frac{4}{3}}\theta_0}{\sin^{\frac{4}{3}}\theta} \varphi(\theta_0) - \varphi(\theta) \right]^{1/2} d\theta \right\}^2, \tag{55}$$

which provides an implicit solution for the position of the spreading front as a function of time $\theta_F(t)$. The dimensionless expression for Eq. (55) is

$$T = \frac{1}{4} \left\{ \int_{\theta_F(t)}^{\theta_0} \sin\theta \left[\frac{\sin^{\frac{4}{3}}\theta_0}{\sin^{\frac{4}{3}}\theta} \varphi(\theta_0) - \varphi(\theta) \right]^{1/2} d\theta \right\}^2. \tag{56}$$

Note that according to Eq. (55), the total time that the film spreads from the initial position of release to the bottom of the hemisphere is

$$t_c = \frac{3\pi^2 \nu R^5}{gV^2} \left\{ \int_{0}^{\theta_0} \sin\theta \left[\frac{\sin^{\frac{4}{3}}\theta_0}{\sin^{\frac{4}{3}}\theta} \varphi(\theta_0) - \varphi(\theta) \right]^{1/2} d\theta \right\}^2, \tag{57}$$

and is a function of the initial position of release θ_0. The dimensionless expression for t_c is

$$T_c \equiv \frac{t_c}{t_0} = \frac{1}{4} \left\{ \int_{0}^{\theta_0} \sin\theta \left[\frac{\sin^{\frac{4}{3}}\theta_0}{\sin^{\frac{4}{3}}\theta} \varphi(\theta_0) - \varphi(\theta) \right]^{1/2} d\theta \right\}^2. \tag{58}$$

As for the thickness of the spreading front, by substituting Eq. (55) into Eq. (53), we get

$$h_F(\theta_F) = \frac{V}{2\pi R^2} \frac{\left[\frac{\sin^{\frac{4}{3}}\theta_0}{\sin^{\frac{4}{3}}\theta_F}\varphi(\theta_0) - \varphi(\theta_F)\right]^{1/2}}{\int_{\theta_F}^{\theta_0} \sin\theta \left[\frac{\sin^{\frac{4}{3}}\theta_0}{\sin^{\frac{4}{3}}\theta}\varphi(\theta_0) - \varphi(\theta)\right]^{1/2} d\theta}. \tag{59}$$

The corresponding dimensionless expression for the thickness of the spreading front is

$$H_F(\theta_F) \equiv \frac{h_F}{h_0} = \frac{\left[\frac{\sin^{\frac{4}{3}}\theta_0}{\sin^{\frac{4}{3}}\theta_F}\varphi(\theta_0) - \varphi(\theta_F)\right]^{1/2}}{\int_{\theta_F}^{\theta_0} \sin\theta \left[\frac{\sin^{\frac{4}{3}}\theta_0}{\sin^{\frac{4}{3}}\theta}\varphi(\theta_0) - \varphi(\theta)\right]^{1/2} d\theta}. \tag{60}$$

Figures 5(a) and 5(b), respectively, show $H_F(\theta_F)$ according to Eq. (60) and $\theta_F(T)$ according to Eq. (56).

Similar to the spreading on a downward-pointing cone, on a lower hemisphere, the film thickness of the spreading front first decreases in time and then increases during the spreading [Fig. 5(a)], due to that the liquid focusing as it flows along the geometry. As a result, there is a minimum of the thickness of the spreading front during the spreading, $h_{F,\min}$. The corresponding position, where the thickness of the spreading front is minimum, is denoted as $\theta_{F,\min}$. Note that both $h_{F,\min}$ and $\theta_{F,\min}$ are dependent on θ_0, the initial position where the liquid is released. The expressions for $h_{F,\min}(\theta_0)$, $\theta_{F,\min}(\theta_0)$, and $t_c(\theta_0)$ are not explicit, but can be calculated numerically; see the results of the numerical calculation in Fig. 6. Also, in the limit of small θ_0 (the initial position of release is close to the bottom), i.e., $\theta_0 \ll 1$, the timescale (note that we give both the dimensional and dimensionless forms)

$$t_c(\theta_0) \sim \frac{3\pi^2 \nu R^5}{4gV^2}\theta_0^4, \quad T_c(\theta_0) \sim \frac{1}{16}\theta_0^4, \tag{61}$$

and the thickness of the spreading front

$$h_F(\theta_F) \sim \frac{V}{\pi R^2} \frac{1}{(\theta_F/\theta_0)^{2/3} - (\theta_F/\theta_0)^2}, \quad H_F(\theta_F) \sim \frac{2}{(\theta_F/\theta_0)^{2/3} - (\theta_F/\theta_0)^2}. \tag{62}$$

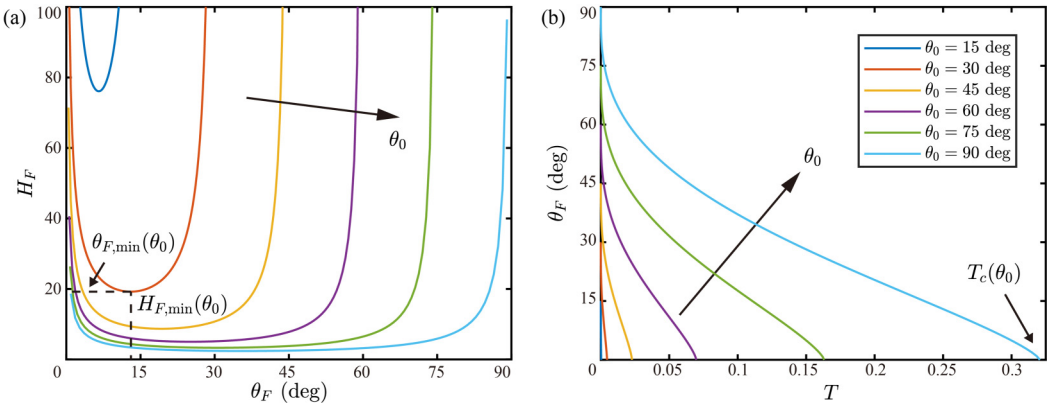

FIG. 5. Gravitational spreading of a viscous thin film on the bottom of a sphere. (a) The scaled thickness of the spreading film front H_F as a function of the position of the spreading film front θ_F. (b) The position of the spreading film front θ_F as a function of the scaled time T.

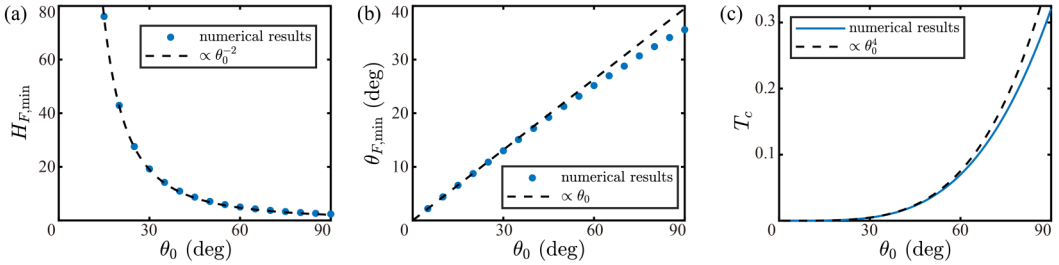

FIG. 6. The characteristic features of spreading on the bottom of a sphere. (a) The scaled minimum value of the film front thickness while spreading, (b) the position where the thickness of the film front is minimum, and (c) the scaled time that the film spreads to the bottom of the sphere, as a function of initial film position of release θ_0. The blue dots and line denote the numerical results and the dashed lines denote the asymptotic curves in the limit of small θ_0, according to Eqs. (61), (63), and (64).

The corresponding position where the thickness of the spreading front is a minimum is

$$\theta_{F,\min}(\theta_0) \sim 3^{-3/4}\theta_0 \approx 0.4387\theta_0, \tag{63}$$

and the corresponding minimum value of the film thickness of the spreading front is

$$h_{F,\min}(\theta_0) \sim \frac{3\sqrt{3}V}{2\pi R^2}\theta_0^{-2}, \quad H_{F,\min}(\theta_0) \sim 3\sqrt{3}\theta_0^{-2}. \tag{64}$$

These asymptotic properties of $t_c(\theta_0)$, $\theta_{F,\min}(\theta_0)$, $h_{F,\min}(\theta_0)$ for small θ_0 agree well with our numerical calculations; see Fig. 6. As for the fingering instability, similar to the scaling argument in the preceding section, the spreading is predicted to be stable when $h_{F,\min} \gtrsim \ell_c$ and is not stable when $h_{F,\min} \lesssim \ell_c$.

IV. EXPERIMENTS

In this section, we report the results of experiments of gravitational spreading on a downward-pointing cone. We focus on measuring $x_F(t)$, the position of the spreading front as a function of time. We also examine the volumetric threshold of the liquid where the fingering instability occurs. A sketch of the experiments is provided in Fig. 7.

A. Experimental setups

Golden syrup (Tate & Lyle) is viscous and approximately Newtonian, and was used in the experiments. The density of the golden syrup $\rho = (1.40 \pm 0.02) \times 10^3\,\mathrm{kg/m^3}$. We measured the viscosity of the syrup using a rheometer (CP50-1, MCR 301, Anton Paar), which confirmed that the syrup behavior is Newtonian and the viscosity $\mu = 40 \pm 2$ Pa s. We then measured the surface tension of the syrup with a pendant droplet method [28] using an in-house Matlab code, yielding surface tension of the syrup $\gamma = 86 \pm 5$ mN/m. Note that our result for the surface tension of the golden syrup is consistent with reported data that $\gamma = 0.08$ N/m [29]. Thus, the corresponding capillary length of the syrup $\ell_c \equiv (\gamma/\rho g)^{1/2} = 2.5$ mm. We measured the material properties of the liquid before and after the experiments and no notable change was observed.

To perform the experiments of gravitational spreading, the golden syrup was placed and released on a funnel. Three funnels (McMaster-Carr) with different sizes were used: the top outer diameters are 26.7, 16.5, and 24.1 cm with cone angles $\alpha = 30$, 30, and 40 degrees, respectively. The axis of symmetry of the cone was oriented vertically, parallel to gravity. In all of the images that are displayed in this article [Figs. 7(c), 7(d), and 8], the top outer diameter of the funnel is 26.7 cm and $\alpha = 30$ degrees.

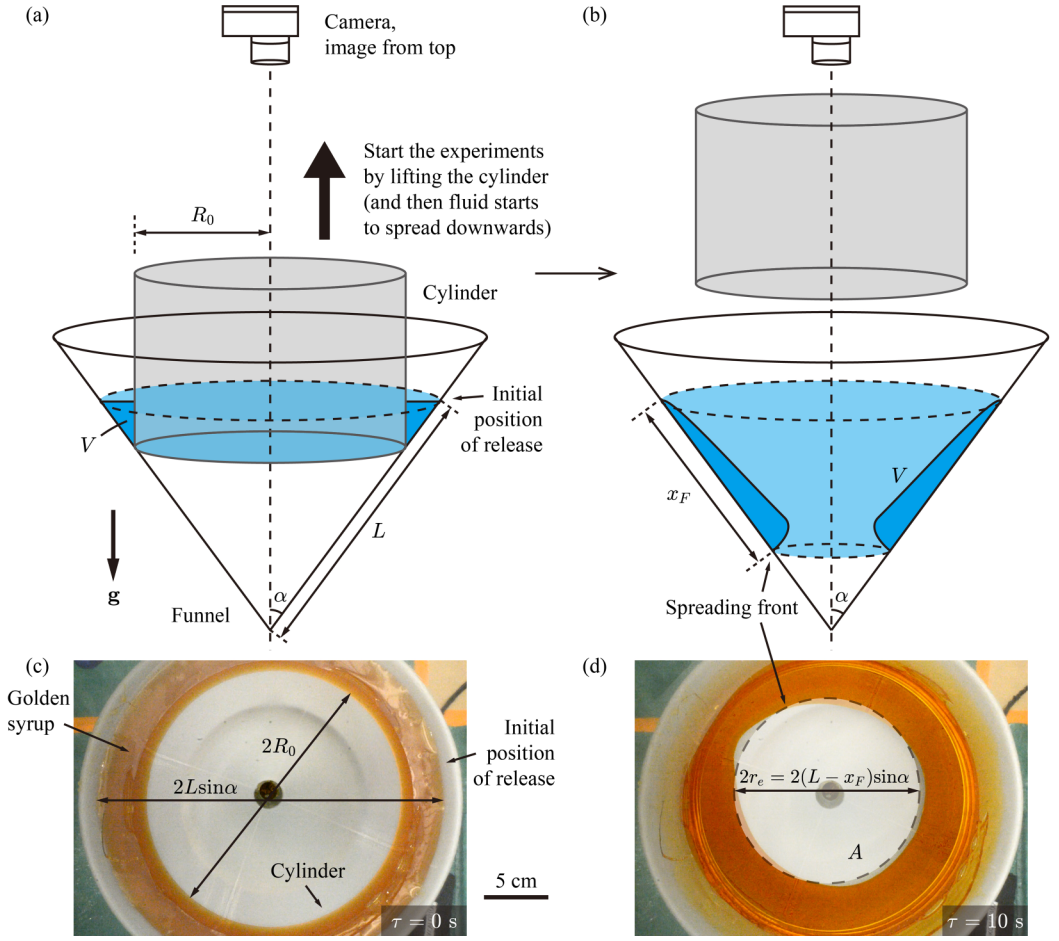

FIG. 7. The sketch of the experiments of gravitational spreading on a funnel. (a) The sketch of the initial condition of the experiments. The experiments start when the cylinder is lifted. (b) The sketch of the experiments while the liquid is spreading. (c) The top view of the initial condition. (d) The top view of the spreading liquid.

To achieve an axisymmetric initial condition, a cylinder was placed on the funnel. Two cylinders (clear cast acrylic tube, McMaster-Carr) with different sizes were used, and the outer radius of the cylinder $R_0 = 10.2$ and 6.4 cm, respectively. The thickness of the tube (the wall of the cylinder) is 0.3 cm and is much smaller than the radius of the cylinder. The axis of symmetry of the cylinder and that of the funnel were collinear. The bottom of the cylinder was in contact with the funnel. Then the golden syrup with a volume of V was poured between the cylinder and the funnel [Fig. 7(a)]. After waiting for several minutes, the surface of the syrup became flat due to gravity and the syrup resembled an axisymmetric liquid ring, which concluded the preparation of the experiment. To start the experiment, at time $\tau = 0$, the cylinder was lifted and the syrup started to spread downwards. Note that τ denotes the time in the experiments. The differences between τ and t will be further described in Sec. IV C. While the cylinder was lifted, there was always a thin liquid film (hanging) between the cylinder and the cone [30], and this hanging film does not significantly affect the spreading and is not the focus of this article. A camera was set on the top of the setup and the images of the spreading were captured [Figs. 7(a) and 7(b)]; see the typical images in Figs. 7(c) and 7(d).

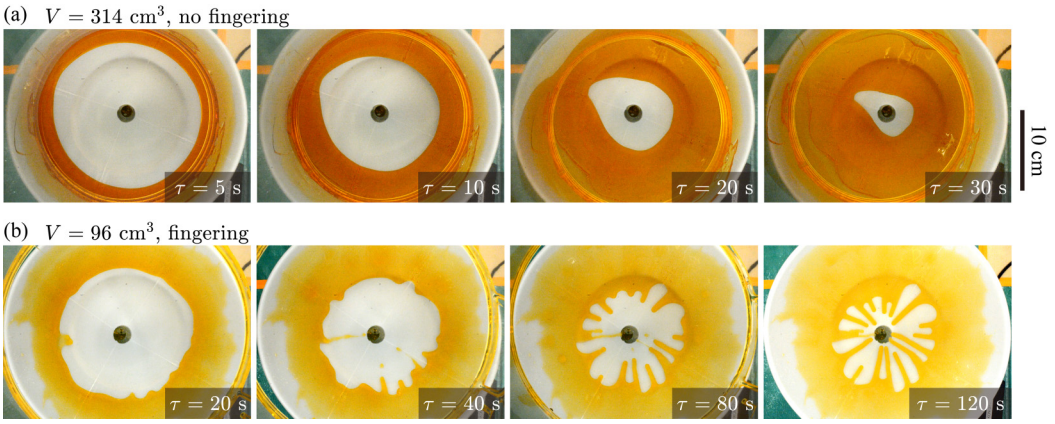

FIG. 8. A time series of the images of spreading. (a) Spreading with no fingering. The total volume of the liquid $V = 314$ cm^3. (b) Spreading with fingering instabilities. $V = 96$ cm^3. See the movies in the Supplemental Material [31]. A scale bar is provided in panel (a).

B. Observations of spreading and instabilities

While spreading without a fingering instability occurring, the spreading front was approximately a circle. We note that the spreading front was usually not perfectly a circle due to the fact that the conditions of the experiment were not perfectly axisymmetric: the setup (funnel or the cylinder) might be slightly tilted and initially there might be more liquid on one side instead of an even axisymmetric distribution. The contact line might also slowly dewet during the spreading. These small nonaxisymmetric effects got amplified during the spreading and therefore the shape of the spreading front deviated from a circle. Nevertheless, this noncircular shape of the spreading front mostly occurred when the spreading front was close to the spout of the funnel, and this effect was not significant so long as we only seek an order-of-magnitude comparison of the measurements to the theoretical predictions. In our measurements, regardless of the exact shape of the spreading front, we calculated the area A that the spreading front enclosed, and then converted this area A to an effective radius of the circle r_e, i.e., $A = \pi r_e^2$, where r_e was the effective radius of the spreading front and was then processed to estimate the position of the spreading front $x_F(t)$ [in particular, $r_e = (L - x_F)\sin\alpha$]; see the sketch of A and r_e in Fig. 7(d).

A fingering instability might occur in the experiments when the volume of the liquid V was relatively small; see the demonstrations in Fig. 8. When the total volume of the liquid V was relatively large [e.g., $V = 314$ cm^3, Fig. 8(a)], the front of the spreading film was stable throughout the spreading and no fingering patterns were observed. In contrast, when V was relatively small [e.g., $V = 96$ cm^3, Fig. 8(b)], the patterns of the spreading film were clearly different: the front of the spreading film became unstable and split into many rivulets. In the experiments, we measured the total volume of the syrup and recorded whether fingering instability was observed on the geometry during the spreading. See the list of the conditions of the experiments in Table II in Appendix B.

C. Measurements and discussions

Next, we focus on analyzing $x_F(t)$, the position of the spreading front as a function of time. In the experiments, we measured and estimated $x_F(\tau)$. Here we want to clarify that the notations of time, t and τ, are different due to the differences between the initial conditions in the model and the experiments: In particular, t is used in the model and $t = 0$ denotes the time when the film starts to spread from the initial position of release, $x_F = 0$. τ is used in the experiments and $\tau = 0$ denotes the time when the cylinder rises and the film starts to spread from the outer diameter of the cylinder, and the initial position of the spreading front in the experiment $x_{F0} = L - R_0/\sin\alpha$ [Fig. 7(c)]. Note

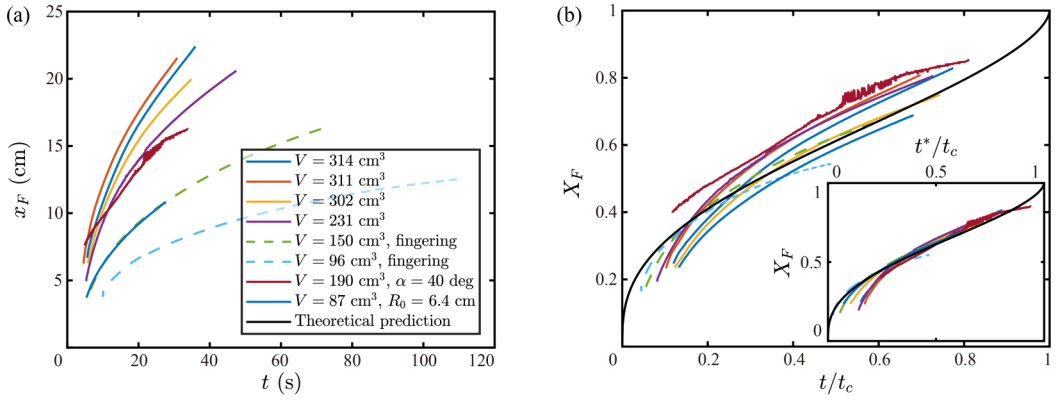

FIG. 9. Experiments for the position of the spreading front on a funnel. (a) The position of the spreading front x_F as a function of time t. (b) The scaled position of the spreading front X_F as a function of the scaled time t/t_c. The angle of the funnel is $\alpha = 30$ degrees and the outer radius of the cylinder $R_0 = 10.2$ cm, unless labeled otherwise. The solid lines (except the black solid line) denote the measurements while no fingering instability was observed. The dashed lines denote the measurements where fingering instabilities were observed. The black line in panel (b) denotes the theoretical prediction $x_F(t/t_c)/L = 1 - [1 - (t/t_c)^{1/3}]^{3/5}$ [Eq. (23)]. The inset shows $X_F(t^*/t_c)$, where $t^* = t + \hat{t}$ and $|\hat{t}|/t_c \approx 0.05$ is a fitting parameter. The initial conditions of the experiments are displayed in Table II in Appendix B (Nos. 1–8).

that the liquid film already occupies a certain amount of the area on the funnel, i.e., from $x = 0$ to x_{F0}. Therefore, the time (or progress) of the spreading is different at $t = 0$ and $\tau = 0$. We focus on the long-time features of the spreading film, when the initial effect of the film shape is negligible. In this limit, the correlation between the time in experiments and the time in the model can be written as

$$t = \tau + t_s, \tag{65}$$

where t_s is the shift of time due to the initial occupation of the liquid film on the funnel. To estimate the value of t_s in the experiments, it can be approximated that the spreading liquid starts to spread from $x_F = 0$ at $t = 0$ and then reaches $x_F = x_{F0}$ at $t = t_s$, which is the initial condition of the experiment (and $\tau = 0$). According to Eq. (23),

$$t_s/t_c = \left[1 - (1 - x_{F0}/L)^{5/3}\right]^3 \approx \left(\frac{5x_{F0}}{3L}\right)^3, \tag{66}$$

where the normalized initial length of the thin film, x_{F0}/L, is small. Given that $x_{F0}/L \approx 0.2$ in the experiments, Eq. (66) indicates that $t_s/t_c = O(10^{-2})$ and is very small; see the values of x_{F0}/L and t_s/t_c in the experiments in Table II in Appendix B. t_c is the timescale given by Eq. (25). According to Eqs. (65) and (66), the measured $x_F(\tau)$ in the experiments can be converted to $x_F(t)$.

In the experiments, we measured $x_F(t)$ with different total volumes of the liquid V, different sizes of the cylinder R_0 and different cone angles α; see the results of (scaled and unscaled) $x_F(t)$ in Fig. 9. As a result, though the unscaled x_F varies significantly with t [Fig. 9(a)], the scaled x_F/L as a function of the scaled time t/t_c collapses to the theoretical prediction Eq. (23) [black line in Fig. 9(b)], which shows good agreement between the experiments and the model. It is also worth pointing out that the averaged position of the spreading front follows the theoretical prediction Eq. (23) even when fingering instabilities were observed (though the average speed of the spreading front is slightly slower when fingering instability occurs).

We note that Eq. (66) is only an estimate of the shift of time t_s since it does not consider the initial thickness profile of the liquid film [for example, in our experiments, the initial thickness

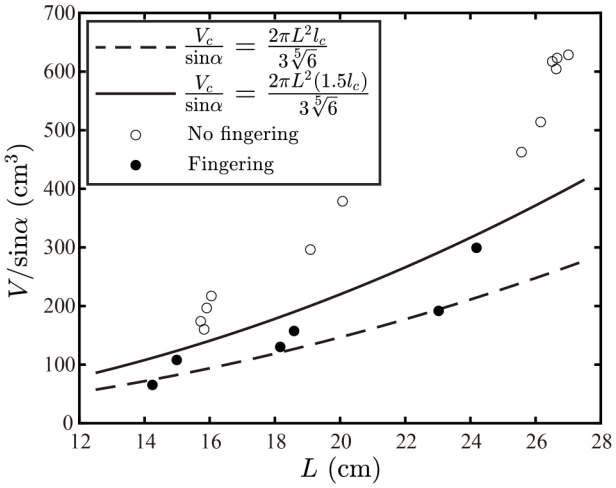

FIG. 10. Determining a critical volume of the fingering instability. The scaled volume of the liquid $V/\sin\alpha$ is displayed as a function of L. The angle of the funnel $\alpha = 30$ or 40 degrees in the experiments. The solid points denote the experiments where fingering was observed. The hollow points denote the experiments where no fingering was observed. The dashed and solid lines denote the theoretical prediction [Eq. (67)] with $c_f = 1$ and $c_f = 1.5$, respectively. We expect the uncertainty of our measurements of the liquid volume V to be within 5%. The initial conditions of the experiments are displayed in Table II in Appendix B (Nos. 1–18).

profile is triangular; see Fig. 7(a)]. To determine t_s requires numerically solving the PDE of the thin film, and is sensitive to the initial condition of the film shape. Though we do not pursue it in this article, further modeling and solving for t_s (as a function of different initial film shapes) remains an interesting topic for future investigations. Since Eq. (66) is only an approximation, we can also apply a translation of t in $X_F(t/t_c)$ in Fig. 9(b); see the inset in Fig. 9(b). A translation of t is applied by $t^* = t + \hat{t}$, where $\hat{t}$ is a fitting parameter for the additional time shift. The average value of $\hat{t}$ among the presented experiments is $|\hat{t}|/t_c \approx 0.05$. As a result, the experimental results agree with the theoretical predictions.

Finally, we estimate the condition of the fingering instability while spreading. In the model, we made a scaling argument for the critical volume of the liquid V_c [Eq. (39)] of the fingering instability. According to the scaling argument,

$$V_c = c_f \frac{2\pi L^2 \ell_c \sin\alpha}{3\sqrt[5]{6}}, \tag{67}$$

where c_f is a constant. Both Eqs. (39) and (67) indicate that $V_c \propto L^2$. In the experiments, we measured the volume of the liquid V, the distance between the top contact line and the vertex of the funnel L (along the generatrix), and recorded whether the fingering instabilities were observed during the spreading; see the results in Fig. 10. The solid points denote the experiments where fingering was observed. The hollow points denote the experiments where no fingering was observed. As a result, the fingering instabilities were observed when the volume of the liquid was relatively small or the distance between the contact line and the vertex of the funnel was relatively large. In practice, we find that Eq. (67) with $c_f = 1.5$ provides a good estimate of the critical volume V_c (the solid line in Fig. 10): fingering instability was observed below this critical volume while the spreading was stable above this critical volume.

V. CONCLUSION

In this article, we studied the gravitational axisymmetric spreading on inclined geometries where the flow converges, in particular, on a downward-pointing cone and on a bowl-shaped hemisphere. We derived expressions for the film thickness profile. At a fixed position, the film thickness $h \propto t^{-1/2}$. Further, we studied the front of the spreading film and derived expressions for the position as well as the thickness of the spreading front. While spreading, the thickness of the spreading front first increases in time and then decreases due to the converging flow. Our major results are summarized in Table I. Also, we calculated the minimum value of the thickness of the spreading front and correlate this value to a fingering instability. Finally, we reported experiments of spreading on an axisymmetric funnel. We measured the position of the spreading front and the critical volume of the fingering instability, and the results are in good agreement with the theoretical predictions. This work highlights the effect of a geometry that focuses the liquid, and provides guidelines for coating on a cone or on a sphere: to achieve a coating without fingering instabilities or rivulets, the total volume of the liquid needs to be larger than a critical value V_c, which depends on geometric parameters, as given approximately by Eq. (67). The onset of the instabilities, the surface tension effects on the spreading (for example, when the scale is as small as the capillary length), and nonaxisymmetric spreading (for example, the spreading of a droplet on a funnel) are some possible topics for future research.

ACKNOWLEDGMENTS

We thank the anonymous referees for their valuable suggestions and recommendations for improvement of the original manuscript. We thank the NSF for support from Grant No. CBET-1804863.

APPENDIX A: AXISYMMETRIC SPREADING ON AN UPWARD-POINTING CONE

Acheson describes the gravitational spreading on an upward-pointing cone, where the position of the spreading front follows $x_F \propto t^{1/5}$ [10]. Here we show the detailed derivations and the results such as the film thickness profile. The derivations are similar to that of the spreading on a downward-pointing cone.

We consider the axisymmetric gravitational spreading of a viscous Newtonian liquid on an upward-pointing cone, with cone angle α; see the sketch in Fig. 11. Initially, at time $t = 0$, liquid with a total volume of V is released on the vertex of the cone. The released liquid then spreads downwards due to gravity, and the distance between the spreading front and the vertex along the

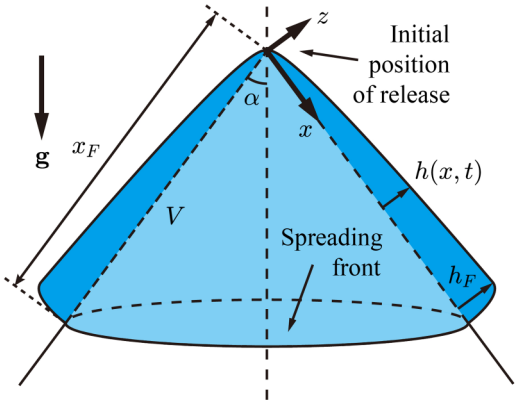

FIG. 11. A sketch of the gravitational spreading of a viscous liquid on an upward-pointing cone.

generatrix is x_F. Similar to the notation of modeling the spreading on a downward-pointing cone [Fig. 1(a)], we denote the direction along the generatrix of the cone as x and the direction orthogonal to the surface of the cone as z, where $x = 0$ represents the vertex of the cone and $z = 0$ represents the surface of the cone. We assume that the spreading of the liquid is axisymmetric and no fingering instability occurs while the liquid spreads.

The velocity profile along the film is parabolic and is the same as Eq. (7). In this geometry, the perimeter of the liquid ring on the cone is $2\pi x\sin\alpha$, and the flow rate is

$$q(x,t) = 2\pi x\sin\alpha \int_0^h u dz = \frac{2\pi g\sin\alpha\cos\alpha}{3\nu} h^3 x. \tag{A1}$$

The PDE for the film thickness $h(x,t)$ is

$$2\pi x\sin\alpha \frac{\partial h}{\partial t} = -\frac{\partial q}{\partial x} = -\frac{2\pi g\sin\alpha\cos\alpha}{3\nu} \frac{\partial (h^3 x)}{\partial x}, \tag{A2}$$

which can be simplified as

$$\frac{\partial h}{\partial t} = -\frac{g\cos\alpha}{3\nu x} \frac{\partial (h^3 x)}{\partial x}. \tag{A3}$$

The solution of Eq. (A3) is similar to the Jeffreys' solution [Eq. (1)],

$$h(x,t) = \left(\frac{3\nu}{5g\cos\alpha}\right)^{1/2} x^{1/2} t^{-1/2}. \tag{A4}$$

This is the expression for the film thickness profile $h(x,t)$; see the thickness profile in Fig. 2(a) (the red line).

The total volume of the liquid V is constant throughout the spreading, thus

$$\int_0^{x_F(t)} 2\pi \sin\alpha x h(x,t) dx = V. \tag{A5}$$

The position of the spreading front can be calculated by substituting Eq. (A4) into Eq. (A5). As a result,

$$x_F = \left(\frac{125 g V^2 \cos\alpha}{48\pi^2 \nu \sin^2\alpha}\right)^{1/5} t^{1/5}, \tag{A6}$$

and the thickness of the spreading front

$$h_F = \left(\frac{9\nu^2 V}{20\pi g^2 \sin\alpha\cos^2\alpha}\right)^{1/5} t^{-2/5} = \frac{5V}{4\pi\sin\alpha} x_F^{-2}; \tag{A7}$$

see the scaled $x_F(t)$ and $h_F(x_F)$ in Fig. 3 (the red lines). Throughout the spreading, the thickness as well as the advancing speed of the spreading front monotonically decrease in time.

APPENDIX B: INITIAL CONDITIONS OF THE EXPERIMENTS

Table II lists the initial conditions and the observations of the experiments. The angle of the funnel α and the outer radius of the cylinder R_0 determined the geometry of the experiments. The volume of the liquid V and the distance between the top contact line of the liquid film and the vertex of the cone along the generatrix L were measured in the experiments. The normalized initial length of the liquid film x_{F0}/L was calculated by $x_{F0}/L = 1 - R_0/(L\sin\alpha)$. The timescale of spreading t_c was calculated by Eq. (25). The time shift between the experiments and the model t_s was calculated by Eq. (66). The values of the fitting parameter $\hat{t}/t_c$ for the inset of Fig. 9(b) are also displayed. The moderate magnitudes of the fitting parameter $\hat{t}/t_c$ are due to the uncertainties in the experimental measurements. Remarks on whether fingering instabilities were observed in the experiments are also

TABLE II. The initial conditions of the experiments. The number of (the trial of) the experiments (No.), the angle of the funnel α, the outer radius of the cylinder R_0, the volume of the liquid V, the distance between the top contact line of the liquid film and the vertex of the cone along the generatrix L, the normalized initial length of the liquid film x_{F0}/L, the timescale of spreading t_c, the normalized time shift between the experiments and the model t_s, the normalized value of the fitting parameter $\hat{t}$, and the remarks on whether fingering instabilities were observed in the experiments, are respectively displayed in the table. Experiment Nos. 1–8 were processed and were used to construct Fig. 9. Experiment Nos. 1–18 were used to construct Fig. 10.

No.	α (deg)	R_0 (cm)	V (cm^3)	L (cm)	x_{F0}/L	t_c (s)	t_s/t_c	$\hat{t}/t_c$	Remark
1	30	10.2	314	27.0	0.25	46	0.05	0.03	No fingering
2	30	10.2	311	26.7	0.24	44	0.05	0.07	No fingering
3	30	10.2	302	26.6	0.24	47	0.05	−0.02	No fingering
4	30	10.2	231	25.6	0.21	65	0.03	0.06	No fingering
5	30	10.2	150	24.2	0.16	118	0.02	0.00	Fingering
6	30	10.2	96	23.0	0.12	225	0.01	−0.02	Fingering
7	40	10.2	190	19.1	0.17	42	0.02	0.12	No fingering
8	30	6.4	87	15.7	0.19	41	0.03	−0.06	No fingering
9	30	10.2	309	26.5	–	–	–	–	No fingering
10	30	10.2	257	26.2	–	–	–	–	No fingering
11	40	10.2	243	20.1	–	–	–	–	No fingering
12	40	10.2	101	18.6	–	–	–	–	Fingering
13	40	10.2	84	18.2	–	–	–	–	Fingering
14	30	6.4	109	16.1	–	–	–	–	No fingering
15	30	6.4	98	15.9	–	–	–	–	No fingering
16	30	6.4	80	15.8	–	–	–	–	No fingering
17	30	6.4	54	15.0	–	–	–	–	Fingering
18	30	6.4	33	14.2	–	–	–	–	Fingering

given in Table II. Note that Experiment Nos. 1–8 were processed and were used to construct Fig. 9. Experiment Nos. 1–18 were used to construct Fig. 10 [Experiment Nos. 9–18 were not processed to track $x_F(t)$].

[1] A. Lee, P.-T. Brun, J. Marthelot, G. Balestra, F. Gallaire, and P. M. Reis, Fabrication of slender elastic shells by the coating of curved surfaces, Nat. Commun. **7**, 11155 (2016).

[2] H. E. Huppert, J. B. Shepherd, R. H. Sigurdsson, and S. J. Sparks, On lava dome growth, with application to the 1979 lava extrusion of the Soufriere of St. Vincent, J. Volcanol. Geotherm. Res. **14**, 199 (1982).

[3] R. W. Griffiths and J. H. Fink, Effects of surface cooling on the spreading of lava flows and domes, J. Fluid Mech. **252**, 667 (1993).

[4] H. E. Huppert and J. E. Simpson, The slumping of gravity currents, J. Fluid Mech. **99**, 785 (1980).

[5] M. Hallworth, H. E. Huppert, and M. Ungarish, On inwardly propagating high-Reynolds-number axisymmetric gravity currents, J. Fluid Mech. **494**, 255 (2003).

[6] M. Ungarish, L. Zhu, and H. A. Stone, Inertial gravity current produced by the drainage of a cylindrical reservoir from an outer or inner edge, J. Fluid Mech. **874**, 185 (2019).

[7] M. Ungarish, *Gravity Currents and Intrusions: Analysis and Prediction*, Vol. 1 (World Scientific, Singapore, 2020).

[8] H. E. Huppert, Flow and instability of a viscous current down a slope, Nature **300**, 427 (1982).

[9] H. Jeffreys, The draining of a vertical plate, Proc. Camb. Phil. Soc. **26**, 204 (1930).

[10] D. J. Acheson, *Elementary Fluid Dynamics* (Oxford University Press, Oxford, UK, 1990).

[11] D. Takagi and H. E. Huppert, Flow and instability of thin films on a cylinder and sphere, J. Fluid Mech. **647**, 221 (2010).
[12] P. D. Howell, H. Kim, M. G. Popova, and H. A. Stone, Rivulet flow over a flexible beam, J. Fluid Mech. **796**, 285 (2016).
[13] J. Gratton and F. Minotti, Self-similar viscous gravity currents: Phase-plane formalism, J. Fluid Mech. **210**, 155 (1990).
[14] J. A. Diez, R. Gratton, and J. Gratton, Self-similar solution of the second kind for a convergent viscous gravity current, Phys. Fluids A: Fluid Dyn. **4**, 1148 (1992).
[15] Z. Zheng, I. C. Christov, and H. A. Stone, Influence of heterogeneity on second-kind self-similar solutions for viscous gravity currents, J. Fluid Mech. **747**, 218 (2014).
[16] Z. Zheng, S. Shin, and H. A. Stone, Converging gravity currents over a permeable substrate, J. Fluid Mech. **778**, 669 (2015).
[17] N. Silvi and E. B. Dussan V, The rewetting of an inclined solid surface by a liquid, Phys. Fluids **28**, 5 (1985).
[18] R. Goodwin and G. M. Homsy, Viscous flow down a slope in the vicinity of a contact line, Phys. Fluids A: Fluid Dyn. **3**, 515 (1991).
[19] T.-S. Lin, J. A. Dijksman, and L. Kondic, Instabilities of a thin liquid film in a funnel, arXiv:2006.14046 (2020).
[20] S. M. Troian, E. Herbolzheimer, S. A. Safran, and J. F. Joanny, Fingering instabilities of driven spreading films, Europhys. Lett. **10**, 25 (1989).
[21] I. Veretennikov, A. Indeikina, and H. C. Chang, Front dynamics and fingering of a driven contact line, J. Fluid Mech. **373**, 81 (1998).
[22] P. H. Trinh, H. Kim, N. Hammoud, P. D. Howell, S. J. Chapman, and H. A. Stone, Curvature suppresses the rayleigh-taylor instability, Phys. Fluids **26**, 051704 (2014).
[23] N. Hammoud, On instabilities in thin-film flows, Ph.D. thesis, Princeton University, 2016.
[24] A. Charogiannis, F. Denner, B. G. M. van Wachem, S. Kalliadasis, B. Scheid, and C. N. Markides, Experimental investigations of liquid falling films flowing under an inclined planar substrate, Phys. Rev. Fluids **3**, 114002 (2018).
[25] G. Lerisson, P. G. Ledda, G. Balestra, and F. Gallaire, Instability of a thin viscous film flowing under an inclined substrate: Steady patterns, J. Fluid Mech. **898**, A6 (2020).
[26] J. R. Lister, Viscous flows down an inclined plane from point and line sources, J. Fluid Mech. **242**, 631 (1992).
[27] N. Xue and H. A. Stone, Self-Similar Draining Near a Vertical Edge, Phys. Rev. Lett. **125**, 064502 (2020).
[28] Y. Rotenberg, L. Boruvka, and A. W. Neumann, Determination of surface tension and contact angle from the shapes of axisymmetric fluid interfaces, J. Colloid Interf. Sci. **93**, 169 (1983).
[29] E. W. Llewellin, H. M. Mader, and S. D. R. Wilson, The rheology of a bubbly liquid, Proc. R. Soc. London A **458**, 987 (2002).
[30] F. Yang and H. A. Stone, Formation, Rupture, and Healing of an Annular Viscous Film, Phys. Rev. Lett. **124**, 224501 (2020).
[31] See Supplemental Material at http://link.aps.org/supplemental/10.1103/PhysRevFluids.6.043801 for the movies that were used to construct Fig. 8 and the descriptions of the movies.